




A sustainable route from kelp to a porous MnO/C network anode for high-capacity lithium-ion batteries

Yanan Zhang¹, Xiaofeng Song¹, Ruitao Huang¹, Youwen Ye¹, Fei Cheng^{1,*} , and Huanrong Li^{1,*}

¹National-Local Joint Engineering Laboratory for Energy Conservation in Chemical Process Integration and Resources Utilization, Tianjin Key Laboratory of Chemical Process Safety, School of Chemical Engineering and Technology, Hebei University of Technology, GuangRong Road 8, Hongqiao District, Tianjin 300130, People's Republic of China

Received: 1 February 2020

Accepted: 13 April 2020

Published online:

23 April 2020

© Springer Science+Business Media, LLC, part of Springer Nature 2020

ABSTRACT

Green and environmentally friendly methods have attracted much attention in the recent research of electrode materials. Natural resources with specific structure and properties are expected to be utilized, and high-performance anodes can be prepared by effectively compounding them with the active components. By choosing kelp with high content of protein as the carbon precursor, a nitrogen-containing MnO/C hybrid with high electrical connectivity has been designed and synthesized. As a kind of seaweed, kelp has an outstanding swelling property in salt solution and its cell membrane is rich in alginate, which is in favor of incorporating and coordinating with Mn^{2+} to form nanosized MnO particles. Moreover, kelp can be used as a template to build the unique network structure, which is conducive to accommodate the volume expansion of MnO during the cycles. The synthesized MnO/C hybrid reveals a superior electrochemical performance when applied to lithium-ion batteries. A high reversible capacity of 978 mAh g^{-1} can be retained at a current density of 0.2 A g^{-1} . This synthesis strategy based on biomass provides a possibility for large-scale preparation of high-capacity electrode materials.

Introduction

The development of electric vehicles, hybrid vehicles and many electronic devices has promoted the researches of the high efficiency energy storage devices [1–3]. Lithium-ion batteries (LIBs) have become the research hot spot in recent years due to their high energy density, faint self-discharge and

long cycling lifespan [4, 5]. Graphite is regarded as the most extensive commercial anode for LIBs because of the stable chemical properties, low charge/discharge potential platform and not obvious volume expansion. However, it cannot adapt to the development of high-energy-density LIBs due to its low theoretical capacity (372 mAh g^{-1}) [6–8]. MnO, as an attractive anode material, has many advantages such as high storage capacity, low cost, abounding in

Address correspondence to E-mail: fcheng@hebut.edu.cn; lihuanrong@hebut.edu.cn

resources and environmental friendliness, which is considered as a potential anode candidate [9, 10]. Nevertheless, MnO is still not satisfactory due to its poor intrinsic conductivity and distinct volume expansion [11–13]. Modification of MnO with carbon is an effective way to improve its electrochemical performance [14–16]. However, traditional carbon modification process is complicated and the morphology is difficult to control. Particles tend to agglomerate and grow up during the high-temperature pyrolysis, which seriously restricts the performance of the battery. In addition, the large-scale preparation of high-performance nano-electrode materials is also a challenge. It is extremely important to develop a facile, cost-effective and environmentally benign method for the synthesis of nanostructured MnO/C anodes.

Plenty of natural resources have a highly interconnected network with developed porous structure, so enabling directional and fast transport. Inspired by nature, a MnO/C hybrid demonstrated a nanoflake network structure was successfully synthesized by using *auricularia* as the carbon precursor and template. The obtained MnO/C anode reveals a reasonable performance of 868 mAh g⁻¹ at 0.2 A g⁻¹ with a good cycle stability [17]. This encouraging result drives us to explore the higher capacity system by taking advantage of the existing structure model in nature.

Herein, we choose an available marine biomass kelp as the carbon precursor and template based on the following advantages: (I) It has a typical cellular structure and a well swelling property in salt solution. High content of manganese salt solution can be incorporated into the kelp cells without destroying the cell structure, and a three-dimensional (3D) network porous structure can be fabricated by the aid of this unique structure model. (II) As a kind of seaweed, kelp has an excellent coordination ability for metal ions [18, 19]. Kelp is rich in alginate, which contains abundant hydroxyl and carboxyl functional groups [20, 21]. Through them, kelp can easily coordinate with Mn²⁺, preventing the agglomeration and growth of MnO nanoparticles during the high-temperature treatment. (III) 8 wt% protein is contained in kelp approximately [22]. The high content of protein will be transformed into the nitrogen-containing carbon during the thermal treatment subsequently, thus improving the electrical conductivity of the hybrid materials. Some electrochemical devices

derived from kelp have been reported [23, 24]. However, it has not been reported as carbon source and template combined with high-capacity transition metal oxide to prepare lithium-ion batteries anode.

Based on the above assumptions, a porous MnO/C hybrid with 3D network structure has been designed via a facile biomass-assisted synthesis route. The coordination of alginate and Mn²⁺ leads to the immobilization of nanosized MnO throughout the highly connected conductive network derived from kelp. This optimal structure benefit from the synergistic effect between the MnO nanoparticles and carbon matrix helps to the infiltration of electrolyte and facilitates the ions diffusion. More importantly, it can effectively buffer the volume expansion of MnO during the charge–discharge process, providing the possibility for a superior long cycling performance. Meanwhile, nitrogen-containing carbon is more favorable for enhancing the electrical conductivity of the hybrid. In addition, this sustainable synthesis method can be extended to other electrode material systems and provides a new idea for large-scale preparation of high-performance electrode materials.

Experimental section

Materials

Manganese chloride tetrahydrate (MnCl₂·4H₂O) and Ammonia (NH₃·H₂O) were purchased from Tianjin Kemiou Chemical Reagent Co., Ltd. The thallus of the kelp *Saccharina japonica* from Rongcheng, Shandong Province, China, was used. All chemical reagents were not further purified before use.

Pretreatment of kelp matrix

Kelp was cut into long strips with a length of 2 cm and a width of 1 cm approximately, which were washed with deionized water. The washed kelp strips were dried at 50 °C for 12 h and named WK. Put the kelp strips in a polypropylene bottle with 20 mL deionized water without contacting directly and then put the sealed bottle in the oven at 120 °C for 2 h. The kelp strips after heat treatment were washed with deionized water for several times and dried at 50 °C for 12 h. The obtained sample was denoted as HWK.

Material synthesis

A certain quality of WK was soaked into 50 mL MnCl_2 solution with a concentration of 1.0 M at 30 °C. After 9 h, the kelp was collected and washed with DI water to rinse the MnCl_2 solution on the surface of kelp. Subsequently, the kelp was put into a Teflon bottle containing ammonia solution (15 wt%), avoiding contacting the ammonia solution directly. Thirdly, the Teflon bottle was heated in an oven at 90 °C for several hours to precipitate the manganese precursor in situ. The product was then washed several times with deionized water and ethanol, and dried at 90 °C for 12 h. Ultimately, the sample was heated at 150 °C for 1 h and 800 °C for 2 h under a heating rate of 5 °C min^{-1} in argon atmosphere. The obtained hybrid was denoted as MC-1. The kelp immersed in MnCl_2 solution with a concentration of 2.3 M and 4.0 M, followed by the same ammonia and heat treatment, could obtain the samples which were named as MC-2 and MC-3. For comparison, the carbon material obtained by pyrolysis from the kelp was denoted as KC. In addition, a MnO/C hybrid named HMC-2 could be obtained by soaking HWK sample in 2.3 M MnCl_2 solution followed by the same ammonia and heat treatment process. In addition, using MC-2 as an anode, the electrochemical performance test was also carried out with the self-made membrane as the separator.

Characterizations

X-ray diffraction (XRD, Bruker D8 Focus, 40 kV, 40 mA, Cu Ka radiation, 1.5418 Å) was performed to analyze the structure of the samples in the 2θ range from 10° to 90°. Raman spectrometer (LabRAM HR Evolution) was used to test with a 532 nm laser excitation. The specific surface area was calculated by using the Brunauer–Emmett–Teller (BET, Micromeritics, ASAP2020M) equation based on the N_2 adsorption–desorption isotherms which were recorded by using a Builder SSA-4200 instrument. The morphologies of the synthesized samples were examined by using the FEI Nova Nano SEM 450 scanning electron microscope (SEM) at an accelerating voltage of 10 kV. The sample for TEM measurements was prepared by smearing the sample dispersion liquid onto a copper grid and dried in air. The thermogravimetric analysis (TGA, SDT2960) of the samples was performed at a heating rate of 10 °C

min^{-1} under air. Fourier transform infrared (FTIR) spectra were obtained with a Bruker Vector 22 spectrometer by using KBr pellets for solid samples from 400 to 4000 cm^{-1} at a resolution of 4 cm^{-1} . Elemental analysis was carried out using an element analyzer (Flash EA1112). X-ray photoelectron spectroscopy (XPS) was obtained by using the spectrometer (ESCALAB 250Xi).

Electrochemical measurements

The active materials, super P and binder (CMC and LA133) were mixed at the weight ratio of 8:1:1 by using deionized water as the solvent to form a slurry. Then, the mixture was coated onto a copper foil and dried at 100 °C for 12 h in a vacuum drying oven. After drying, the loaded Cu foil was cut into disk electrodes with a diameter of 12 mm and calendered at 10.0 MPa. The mass loading of the active material on each disk electrodes was close to 1 mg. CR2025 coin-type cells were used to assemble in an argon-filled glove box. The electrolyte is a solution of 1.0 M LiPF_6 in mixed dimethyl carbonate (DMC), ethyl methyl carbonate (EMC) and ethylene carbonate (EC) (1:1:1, v/v/v). Lithium metal was used as the counter electrode and Celgard 2400 membrane as the separator, respectively.

The galvanostatic charge–discharge measurements were delivered on a LAND CT2001A battery test system from 0.01 to 3.0 V (vs. Li/Li^+) at room temperature. The cyclic voltammetry (CV) measurements of the cells were carried out on a CHI660E electrochemical workstation at a scan rate of 0.1 mV s^{-1} . The electrochemical impedance spectroscopy (EIS) was conducted in the frequency range from 10^5 to 10^{-2} Hz. Each assembled coin cell was set still for 12 h before the test.

Results and discussion

The preparation process of the 3D honeycomb-like porous MnO/C hybrid is shown in Fig. 1. As a common marine organism, kelp has been proved to have a good swelling property in salt solutions. After immersion in MnCl_2 solution at 25 °C for nine hours, the volume and weight of kelp increased significantly (see Fig. S1). In addition, Mn^{2+} coordinated with carboxyl and hydroxyl groups in alginate and immobilized in kelp cells during the immersion

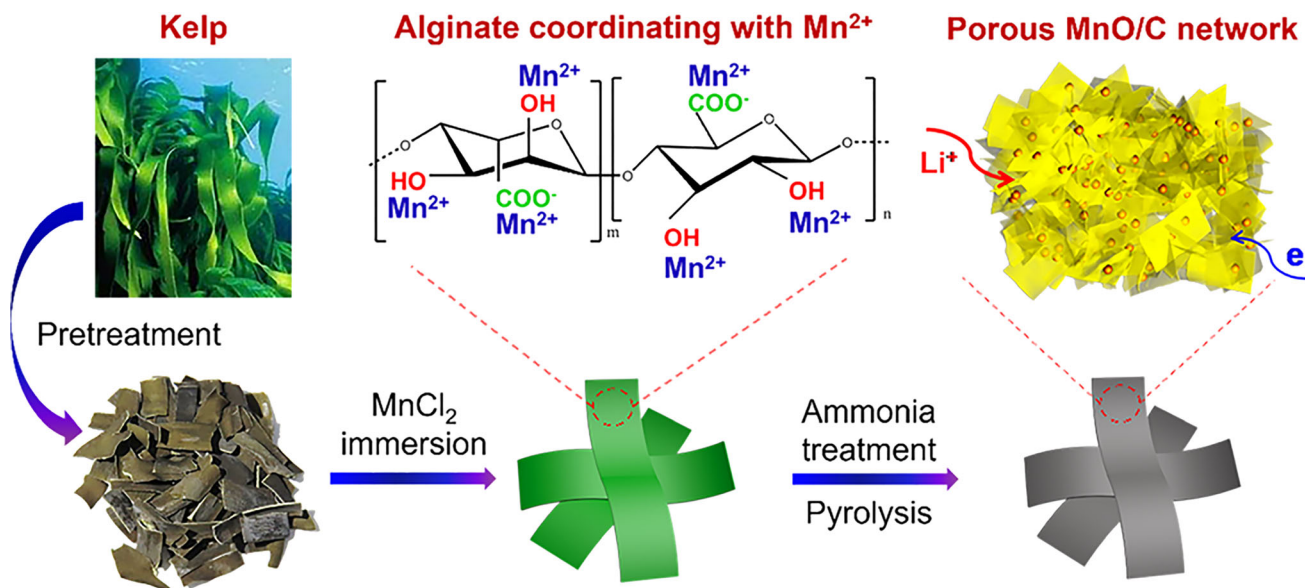


Figure 1 Schematic illustration of the porous MnO/C hybrid.

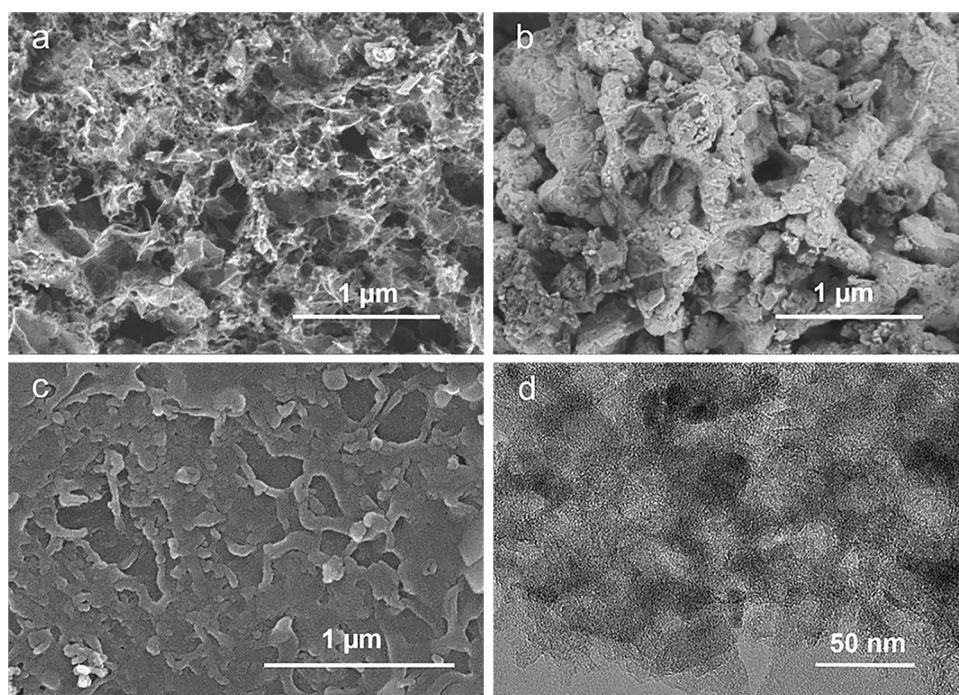
process. After an ammonia treatment at 90 °C and subsequent carbonization at 800 °C, MnO nanoparticles are in situ produced and encapsulated into the carbon network.

As a kind of seaweeds, kelp has an excellent ability to coordinate with metal ions because the cell membrane of kelp is rich in alginate [21]. The functional groups of kelp matrix were analyzed by FTIR. FTIR curve has characteristic peaks at 1045, 1384, 1627, 2920 and 3434 cm^{-1} which corresponds to $-\text{C}-\text{O}$, $-\text{C}=\text{O}$, $-\text{COO}$, $-\text{CH}$ and $-\text{OH}$ groups in alginate, respectively, as shown in Fig. S2. When kelp was immersed in MnCl_2 solution, a large number of carboxyl and hydroxyl groups in alginate provide good coordination sites for Mn^{2+} , which effectively preventing the growth of nanoparticles during the subsequent high-temperature treatment process. The molecular structure and properties of alginate can be destroyed with the removing of bound water in molecular beginning at 60 °C. According to this property, we kept the kelp at high temperature of 120 °C for 2 h to destroy the alginate and explored the influence of alginate on the preparation of MnO/C hybrid.

Figure 2a shows the microstructure of the MnO/C hybrid (MC-2) which exhibits a honeycomb-like 3D porous network structure. This kind of porous network structure can provide enough buffer space for the volume expansion of MnO during the charge-discharge process. Meanwhile, this 3D cross-linked

structure can effectively improve the electrical connectivity of the hybrid. Similar to the structure of MC-2, MC-1 and MC-3 prepared by changing the concentration of MnCl_2 solution also exhibit the 3D network structure (Fig. S3a, b). To investigate the effect of alginate on the structure of the hybrid, the morphology of HMC-2 was observed by SEM (Fig. 2b). Different from MC-2, HMC-2 shows a not obvious network feature without the confinement of alginate, and the synthesized MnO particles tend to agglomerate and grow up. Therefore the cooperation of kelp matrix and Mn^{2+} plays an important role in the formation of this unique network structure. The TEM image of HMC-2 also proves the vital effect of alginate on the formation of 3D network structure (Fig. S4). It can be seen from the image that some MnO particles in HMC-2 hybrid are exposed outside the carbon matrix and not be coated completely without the alginate during the preparation process. The morphology of carbon by pyrolysis of kelp (KC) is shown in Fig. 2c which has a rough surface. The morphology of MC-2 was also examined by TEM. As shown in Fig. 2d, the MnO nanoparticles are immobilized in the carbon skeleton uniformly. The MnO particles dispersed without obvious agglomeration also verifies that the strategy of in situ preparation of non-agglomerated metal oxides derived from kelp is feasible. In addition, the TEM image of MC-2 also exhibits a porous structure. TEM image of MC-2 and the particle size distribution of MnO nanoparticles

Figure 2 SEM images of **a** MC-2, **b** HMC-2, **c** KC and **d** TEM image of MC-2.



are shown in Fig. S5. The particle size analysis of TEM shows that MnO nanoparticles are mainly distributed in the range of 22–34 nm.

XRD is performed to reveal the crystallographic structures of the products. As illustrated in Fig. 3a, the diffraction peaks of MC-1, MC-2 and MC-3 at 2θ of 34.9° , 40.5° , 58.7° , 70.1° and 73.8° correspond to the (111), (200), (220), (311) and (222) planes of MnO (JCPDS card No. 07-0230) [25]. Received by XRD Rietveld refinement method, the full width at half maximum (FWHM) of the (200) peak for MC-1, MC-2 and MC-3 was 0.236, 0.212 and 0.148. The average sizes of MnO nanocrystals for MC-1, MC-2 and MC-3 are 35, 39 and 56 nm, respectively, which are analyzed by the Scherrer formula from the (200) peak. The XRD patterns reveal that the kelp-derived carbon (KC) owns two broad peaks located at around 23° and 44° , corresponding to (002) and (101), demonstrating the presence of graphitic carbon [26, 27]. This result can also be verified by Raman spectra (Fig. 3b). The two obvious peaks located at 1352 and 1602 cm^{-1} can be ascribed to the disordered carbon (D-band) and the ordered graphitic carbon (G-band), respectively. And the I_D/I_G ratio of MC-1, MC-2, MC-3 and KC composites are calculated as 0.96, 0.97, 0.95 and 1.07, suggesting a relatively high degree of graphitization [28].

It is noted that with the variation of the MnCl_2 solution concentration, the swelling capacity of kelp is changed, which can be confirmed by TGA. Figure 3c shows the TGA curves of MC-1, MC-2 and MC-3 under air from room temperature to 900°C . XRD pattern of the annealed MC-2 sample under air condition at 900°C indicates that MnO was oxidized to Mn_3O_4 (Fig. S6). Therefore, the major weight change is caused by the decomposition of carbon skeleton and the oxidation of MnO [29]. The TGA curves illustrate that the corresponding MnO contents are calculated to be 51.5 wt% (MC-1), 49.2 wt% (MC-2) and 46.4 wt% (MC-3), respectively. During the process of material preparation, after being immersed in MnCl_2 solution, kelp was washed with deionized water to clean the Mn^{2+} on the surface of kelp. With the content of manganese salt solution increasing, the content of MnO is gradually decreasing based on TGA, which may be because the swelling of kelp is related to the concentration of salt solution. When the kelp is immersed in low concentration solution, a large number of Mn^{2+} enter kelp cells to form MnO nanoparticles after ammonia and heat treatment, resulting in a high content of MnO loading in MC-1 hybrid. However, in the high concentration solution (4 M), the swelling property of kelp was inhibited, resulting in a small amount of MnO loading in MC-3 hybrid.

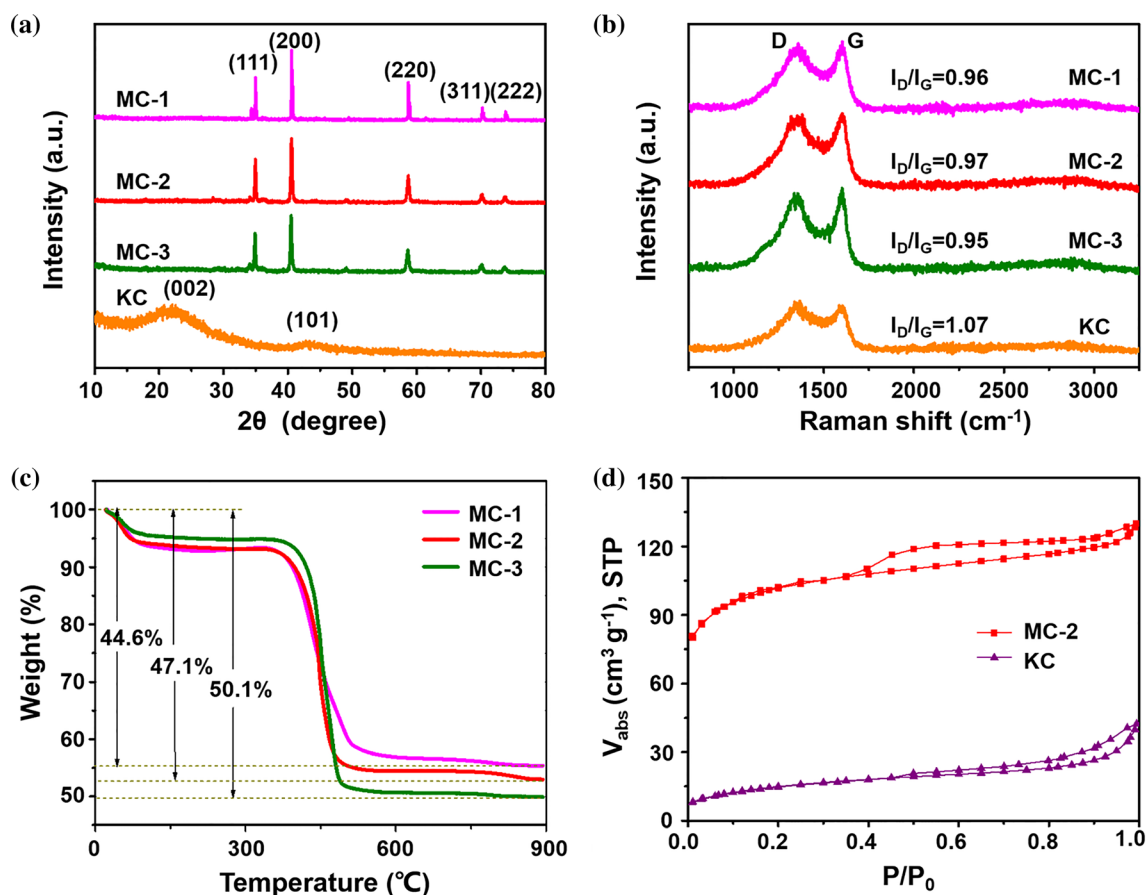


Figure 3 **a** XRD patterns of MC-1, MC-2, MC-3 and KC, **b** Raman spectra, **c** TGA curves of MC-1, MC-2 and MC-3 under air from room temperature to 900 °C and **d** N₂ adsorption–desorption isotherms of KC and MC-2.

The TEM image of MC-2 exhibits a porous structure, which can also be verified by nitrogen sorption at 77 K. The specific surface areas of MC-2 and KC (Fig. 3d) are 349 and 55 m² g⁻¹, respectively. The pore size (Fig. S7) of MC-2 focus in the range of 1.89 and 3.58 nm and the pore size of KC focus in the range of 1.73 and 3.88 nm. The formation of mesoporous is due to the interaction between MnO and the carbon matrix during pyrolysis. The nitrogen content measured by elemental analysis is 2.6 wt%, which can be attributed to the high content protein in kelp.

XPS spectra confirmed the presence of C, N, O and Mn in MC-2 hybrid (Fig. 4a). The peaks of Mn 2*p*, N 1*s*, and C 1*s* have been further analyzed by high-resolution XPS. The high-resolution Mn 2*p* XPS spectrum, as shown in Fig. 4b, has two main peaks that can be attributed to Mn 2*p*_{3/2} peak at 641.6 eV and Mn 2*p*_{1/2} peak at 653.7 eV, which are the characteristic peaks of MnO. The two satellite peaks on

the higher binding-energy sides can be attributed to the hybridization between the Mn 3*d* and other valence orbitals [30, 31]. The high-resolution N 1*s* XPS spectrum of MC-2 (Fig. 4c) can be deconvoluted into three peaks at 397.9, 399.6 and 401.8 eV, interpreting as the pyridinic, pyrrolic and graphitic types of N atoms, respectively [32, 33]. This further proves the existence of nitrogen in the MnO/C hybrid. The C 1*s* XPS spectrum of MC-2 hybrid is shown in Fig. 4d. The peaks at 284.6, 285.3, 286.5 and 289.1 eV can be attributed to C–C, C–N, C–O and O=C–O, respectively [34].

To evaluate the electrochemical performances of as prepared electrodes, the samples were tested as anode for LIBs. The CV curves of MC-2 for the first three consecutive cycles at the scan rate of 0.1 mV s⁻¹ are shown in Fig. 5a. The main cathodic peaks appearing at 0.25 V and 0.75 V, respectively, in the first discharge process can be interpreted to the reduction reaction of MnO to metallic Mn and

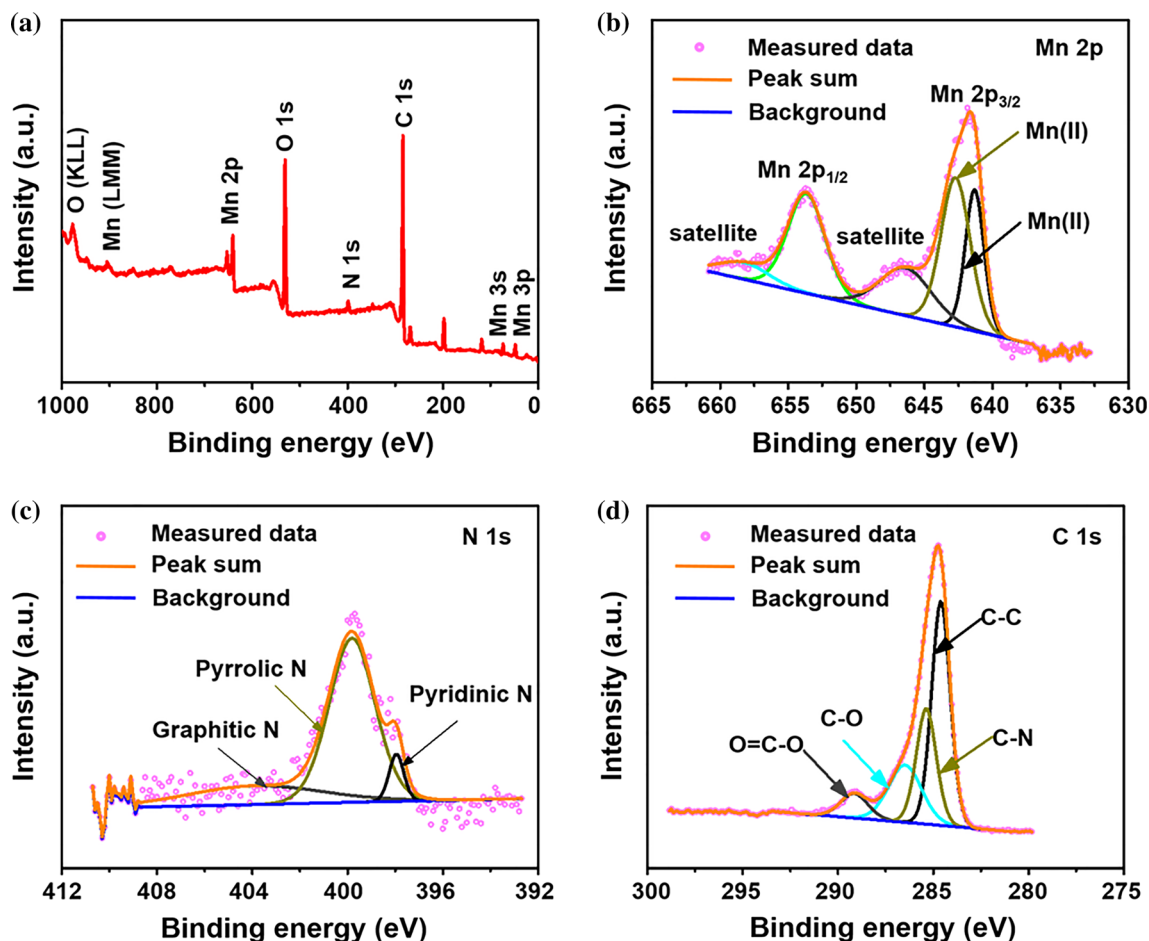


Figure 4 XPS spectra of MC-2, **a** survey scan, **b** Mn 2p, **c** N 1s, **d** C 1s.

formation of the solid electrolyte interphase (SEI) film on the electrode surface [3]. The anodic peak at 1.27 V is the oxidation from metallic Mn to MnO and the decomposition of Li_2O [29]. In the next two cycles, the cathodic peak at 0.25 V shifts to 0.48 V suggesting the formation of the stable SEI layer and the improved kinetics in the following cycles [12, 34]. In addition, the peaks coincide in the subsequent cycles, suggesting the good cycling performance of the electrode.

Figure 5b and c shows the constant current charge–discharge curves and the cycling performance of all the samples, which were carried out at a current density of 0.2 A g^{-1} between the potential range from 0.01 to 3 V (vs. Li/Li^+). The specific capacity is calculated based on the total mass of the active materials (MnO/C). The discharge and charge capacity for MC-2 in the first cycle is 1570 and 778 mAh g^{-1} . The irreversible capacity in the first cycle is mainly interpreted as the formation of the SEI layer and the

decomposition of electrolyte. Compared with sample MC-1, MC-3 and KC, MC-2 shows a much higher capacity and cycling performance. After 250 cycles, the reversible discharge capacity reaches 978 mAh g^{-1} , which drastically exceeds the theoretical capacity of MnO. This superior capacity upon cycling may be related to the reoxidation of Mn^{2+} to higher oxidation states in the MnO/C-based anode materials due to the synergistic effect of carbon and MnO [35]. In order to further study the contribution of alginate in help to the electrochemical performance, we intentionally used high-temperature treatment to destroy the alginate in kelp cells and the MnO/C hybrid (HMC-2) was synthesized by using this matrix. As shown in Fig. 5c, in the first 100 cycles, HMC-2 exhibits a similar reversible capacity to that of MC-2. However, after 100 cycles, the capacity of HMC-2 decreases rapidly, which may be due to the structural collapse of the MnO/C hybrid. Without the coordination of alginate, Mn^{2+} can

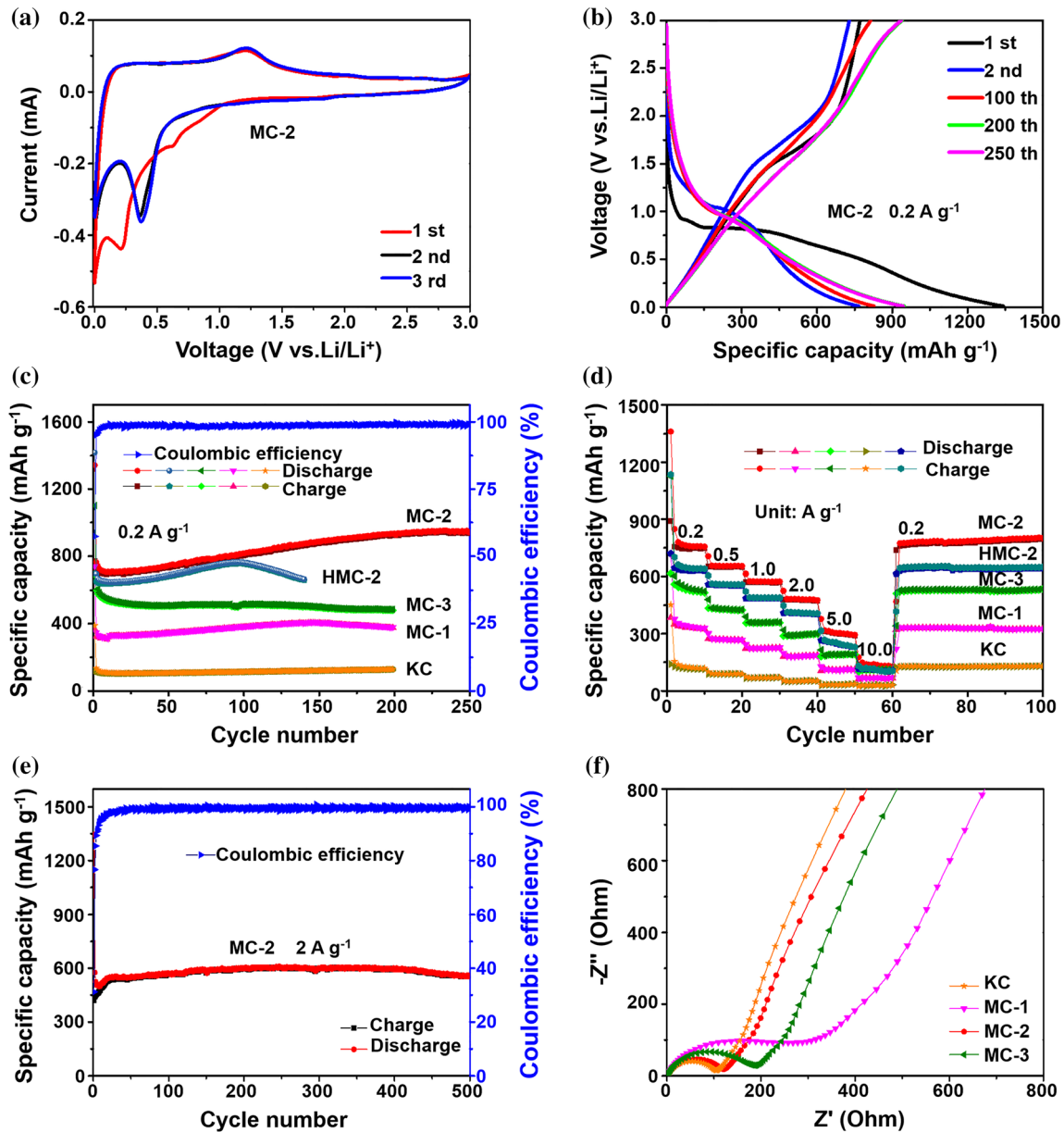


Figure 5 a CV curves of the MC-2 hybrid at 0.1 mV s⁻¹ for first three cycles, b charge–discharge profiles of MC-2 at the current density of 0.2 A g⁻¹ for 1st, 2nd, 100th, 200th and 250th cycles in

the potential window of 0.01–3.0 V. c Cycling performances, d rate capability, e long cycling performance at 2 A g⁻¹ and f electrochemical impedance spectra.

hardly be immobilized in the kelp cells. The MnO nanoparticles are easy to grow up due to the lack of confinement, resulting in large volume change and capacity fading during cycles. This result further demonstrates that besides the swelling property, the coordination of kelp and Mn²⁺ is the key to obtain the nanosized MnO dispersed highly conductivity network.

The rate capability of MC-1, MC-2, MC-3, HMC-2 and KC was also measured at various current

densities from 0.2 to 10.0 A g⁻¹ (Fig. 5d). The capacities of MC-2 are 762, 660, 578, 485 and 311 mAh g⁻¹ at 0.2, 0.5, 1.0, 2.0 and 5.0 A g⁻¹, respectively. Even at 10.0 A g⁻¹, the MC-2 hybrid also delivers a capacity of 139 mAh g⁻¹. When the current density recovers to 0.2 A g⁻¹, the capacity of the MC-2 electrode is back to initial level, suggesting that the highly connected structure of MnO/C hybrid preserves the integrity of the electrode and thus enables it to tolerate different charge and discharge

currents. Compared with HMC-2, the rate performance of MC-2 is better than that of HMC-2, which proves that the alginate in kelp is contribute to the improvement of electrochemical performance. The improved cycling stability and high reversible capacity demonstrate that the 3D network structure can buffer the huge volume change during charging/discharging, which is also confirmed by SEM (Fig. S8). The SEM image exhibits a porous connected structure with a rough surface. The rough surface may be the SEI generated during the first cycle, which may help to keep the structure stable and improve the cyclic stability of MC-2 [36, 37]. To further test its high-power applications of rechargeable batteries, the long-cycling performance at a high current density of 2 A g^{-1} was executed, as shown in Fig. 5e. Over 500 cycles, MC-2 still retains a high average discharge capacity of 554 mAh g^{-1} , indicating a high cycling and rate performance. Compared with other MnO/C anodes reported previously, MC-2 exhibits a superior electrochemical performance which is compared in Table S1 (supporting information) [37–45]. The Nyquist plots of MC-1, MC-2, MC-3 and KC samples are shown in Fig. 5f. The corresponding equivalent circuit is shown in Fig. S9, and the results are summarized in Table S2. Compared with that of MC-1 and MC-3, a distinctly smaller semicircle in the high-frequency region of the impedance spectra is observed for MC-2, which is close to that of the pure carbon (KC), indicating the rapid transport of electrons and lithium ions in our synthesized MnO/C hybrid, thus resulting in improved cycling and rate performance. In addition, we used self-made separator to assemble the battery and tested the electrochemical performance of MC-2. The battery assembly and testing conditions are consistent with the previous batteries. As shown in Fig. S10, the discharge/charge capacity in the first cycle is $1270/1124 \text{ mAh g}^{-1}$ with an improved ICE of 88.5%. Over 50 cycles, it can still retain a high reversible capacity with a coulombic efficiency higher than 99%, indicating a superior electrochemical performance.

Conclusions

Benefiting from the swelling property and structural advantages of kelp, a 3D porous network-structure MnO/C hybrid is obtained via a facile biomass-assisted synthesis method. The prepared nanosized

MnO particles are uniformly dispersed and encapsulated in the nitrogen-containing carbon network because of the coordination between alginate and Mn^{2+} as well as high content of protein in kelp. The obtained optimal structure not only has good electrical connectivity, but also can effectively alleviate the volume expansion of MnO during the cycles. When applied to the anode for LIBs, it shows an excellent electrochemical performance, suggesting that this structure is conducive to the rapid transmission of lithium ions and electrons. In addition, this sustainable synthesis strategy provides a new idea for the large-scale preparation of high-performance electrode materials for LIBs.

Supplementary material

The photograph of kelp matrix (WK) before and after immersion. FTIR curve of WK. SEM images of MC-1 and MC-3. XRD pattern of Mn_3O_4 . The pore-size distribution plot from the adsorption branch isotherm calculated by the BJH method. Electrochemical performance of MC-2 using self-made separator. Electrochemical performance of some comparable MnO anodes.

Acknowledgements

Financial support by the National Natural Science Foundation of China (21805067) and Colleges and Universities in Hebei Province Science and Technology Research Project (QN2018045).

Author's contribution

The manuscript was written through contributions of all authors. All authors have given approval to the final version of the manuscript.

Compliance with ethical standards

Conflict of interest The authors declare that they have no conflict of interest.

Electronic supplementary material: The online version of this article (<https://doi.org/10.1007/s10853-020-04680-w>) contains supplementary material, which is available to authorized users.

References

- [1] Goodenough JB, Park K-S (2013) The Li-ion rechargeable battery: a perspective. *J Am Chem Soc* 135:1167–1176
- [2] Li H, Wang Z, Chen L, Huang X (2009) Research on advanced materials for Li-ion batteries. *Adv Mater* 21:4593–4607
- [3] Bruce PG, Scrosati B, Tarascon JM (2008) Nanomaterials for rechargeable lithium batteries. *Angew Chem Int Ed* 47:2930–2946
- [4] Chu Y, Guo L, Xi B et al (2017) Embedding MnO@Mn₃O₄ nanoparticles in an N-doped-carbon framework derived from Mn-Organic clusters for efficient lithium storage. *Adv Mater* 30:1704244
- [5] Qu X, Zhang X, Gao Y, Hu J, Gao M, Pan H, Liu Y (2019) Remarkably improved cycling stability of boron-strengthened multicomponent layer protected micron-Si composite anode. *ACS Sustain Chem Eng* 7:19167–19175
- [6] Cui Z, Liu Q, Xu C et al (2017) A new strategy to effectively alleviate volume expansion and enhance conductivity of hierarchical MnO@C nanocomposites for lithium ion batteries. *J Mater Chem A* 5:21699–21708
- [7] Li W, An C, Guo H et al (2019) In situ synthesis of 1D mesoporous MnO@C nanorods for high performance Li-ion batteries. *ACS Sustain Chem Eng* 7:139–146
- [8] Zhou X, Yu L, Lou X (2016) Nanowire-templated formation of SnO₂/carbon nanotubes with enhanced lithium storage properties. *Nanoscale* 8:8384–8389
- [9] Bai T, Zhou H, Zhou X, Liao Q, Chen S, Yang J (2017) N-doped carbon-encapsulated MnO@graphene nanosheet as high-performance anode material for lithium-ion batteries. *J Mater Sci* 52:11608–11619. <https://doi.org/10.1007/s10853-017-1247-7>
- [10] Gao J, Lowe MA, Abruna HD (2011) Spongelike nanosized Mn₃O₄ as a high-capacity anode material for rechargeable lithium batteries. *Chem Mater* 23:3223–3227
- [11] Guo S, Lu G, Qiu S et al (2014) Carbon-coated MnO microparticulate porous nanocomposites serving as anode materials with enhanced electrochemical performances. *Nano Energy* 9:41–49
- [12] Jiang H, Hu Y, Guo S, Yan C, Lee PS, Li C (2014) Rational design of MnO/carbon nanopeapods with internal void space for high-rate and long-life Li-ion batteries. *ACS Nano* 8:6038–6046
- [13] Sun B, Chen Z, Kim H-S, Ahn H, Wang G (2011) MnO/C core-shell nanorods as high capacity anode materials for lithium-ion batteries. *J Power Sources* 196:3346–3349
- [14] Cheng F, Li W-C, Lu A-H (2016) Using confined carbonate crystals for the fabrication of nanosized metal oxide@carbon with superior lithium storage capacity. *J Mater Chem A* 4:15030–15035
- [15] Xiao Y, Cao M (2015) Carbon-anchored MnO nanosheets as an anode for high-rate and long-life lithium-ion batteries. *ACS Appl Mater Interfaces* 7:12840–12849
- [16] Liu D-H, Lü H-Y, Wu X-L et al (2015) Constructing the optimal conductive network in MnO-based nano hybrids as high-rate and long-life anode materials for lithium-ion batteries. *J Mater Chem A* 3:19738–19746
- [17] Cheng F, Li W-C, Lu A-H (2016) An interconnected nanoflake network derived from a natural resource for high-performance lithium-ion batteries. *ACS Appl Mater Interfaces* 8:27843–27849
- [18] Holan ZR, Volesky B (1994) Biosorption of lead and nickel by biomass of marine-algae. *Biotechnol Bioeng* 43:1001–1009
- [19] Murphy V, Hughes H, McLoughlin P (2007) Cu (II) binding by dried biomass of red, green and brown macroalgae. *Water Res* 41:731–740
- [20] Zhang H, Zong P, Chen M et al (2019) In situ synthesis of multilayer carbon matrix decorated with copper particles: enhancing the performance of Si as anode for Li-ion batteries. *ACS Nano* 13:3054–3062
- [21] Yun Y-S, Park D, Park JM, Volesky B (2011) Biosorption of trivalent chromium on the brown seaweed biomass. *Environ Sci Technol* 35:4353–4358
- [22] Kim E-Y, Kim D-G, Kim Y-R, Hwang H-J, Nam T-J, Kong I-S (2011) An improved method of protein isolation and proteome analysis with *Saccharina japonica* (Laminariales) incubated under different pH conditions. *J Appl Phycol* 23:123–130
- [23] Sun N, Li Z, Zhang X et al (2019) Hierarchical porous carbon materials derived from kelp for superior capacitive applications. *ACS Sustain Chem Eng* 7:8735–8743
- [24] Hei Y, Li X, Zhou X et al (2018) Electrochemical sensing platform based on kelp-derived hierarchical meso-macroporous carbons. *Anal Chim Acta* 1003:16–25
- [25] Liu C, Zhang C, Song H, Zhang C, Liu Y, Nan X, Cao G (2016) Mesocrystal MnO cubes as anode for Li-ion capacitors. *Nano Energy* 22:290–300
- [26] Zhou Y, Candelari SL, Liu Q, Uchaker E, Cao G (2015) Porous carbon with high capacitance and graphitization through controlled addition and removal of sulfur-containing compounds. *Nano Energy* 12:567–577
- [27] Liu D-S, Liu D-H, Hou B-H, Wang Y-Y, Guo J-Z, Ning Q-L, Wu X-L (2018) 1D porous MnO@N-doped carbon nanotubes with improved Li-storage properties as advanced anode material for lithium-ion batteries. *Electrochim Acta* 264:292–300

- [28] Gan Q, He H, Zhao K, He Z, Liu S (2018) Preparation of N-doped porous carbon coated MnO nanospheres through solvent-free in situ growth of ZIF-8 on ZnMn_2O_4 for high-performance lithium-ion battery anodes. *Electrochim Acta* 266:254–262
- [29] Zhang C, Wang J-G, Jin D, Xie K, Wei B (2015) Facile fabrication of MnO/C core-shell nanowires as an advanced anode material for lithium-ion batteries. *Electrochim Acta* 180:990–997
- [30] Liu C, Zhang C, Fu H, Nan X, Cao G (2017) Exploiting high-performance anode through tuning the character of chemical bonds for Li-ion batteries and capacitors. *Adv Energy Mater* 7:1601127
- [31] Guo D, Wu Z, An Y et al (2015) Room temperature ferromagnetism in $(\text{Ga}_{1-x}\text{Mn}_x)_2\text{O}_3$ epitaxial thin films. *J Mater Chem C* 3:1830–1834
- [32] Zhu G, Chen T, Hu Y et al (2017) Recycling $\text{PM}_{2.5}$ carbon nanoparticles generated by diesel vehicles for supercapacitors and oxygen reduction reaction. *Nano Energy* 33:229–237
- [33] Niu W, Li Z, Marcus K et al (2018) Surface-modified porous carbon nitride composites as highly efficient electrocatalyst for Zn-air batteries. *Adv Energy Mater* 8:1701642
- [34] Leon V, Quintana M, Herrero MA, Fierro JLG, Hoz A, Prato M, Vazquez E (2011) Few-layer graphenes from ball-milling of graphite with melamine. *Chem Commun* 47:10936–10938
- [35] Sun Y, Hu X, Luo W, Xia F, Huang Y (2013) Reconstruction of conformal nanoscale MnO on graphene as a high-capacity and long-life anode material for lithium ion batteries. *Adv Funct Mater* 23:2436–2444
- [36] Jiang X, Yu W, Wang H, Xu H, Liu X, Ding Y (2016) Enhancing the performance of MnO by double carbon modification for advanced lithium-ion battery anodes. *J Mater Chem A* 4:920–925
- [37] Zhu G, Wang L, Lin H et al (2018) Walnut-like multicore-shell MnO encapsulated nitrogen-rich carbon nanocapsules as anode material for long-cycling and soft-packed lithium-ion batteries. *Adv Funct Mater* 28:1800003
- [38] Lin Y, Zhao S, Qian J et al (2020) Petal cell-derived MnO nanoparticle-incorporated biocarbon composite and its enhanced lithium storage performance. *J Mater Sci* 55:2139–2154. <https://doi.org/10.1007/s10853-019-04085-4>
- [39] Guo Y, Zheng L, Lan J-L, Yu Y, Yang X (2018) MnO nanoparticles encapsulated in carbon nanofibers with sufficient buffer space for high-performance lithium-ion batteries. *Electrochim Acta* 269:624–631
- [40] Wang J-G, Liu H, Liu H, Fu Z, Nan D (2017) Facile synthesis of microsized MnO/C composites with high tap density as high performance anodes for Li-ion batteries. *Chem Eng J* 328:591–598
- [41] Mu P, Ma W, Zhao Y et al (2019) Facile preparation of MnO/nitrogen-doped porous carbon nanotubes composites and their application in energy storage. *J Power Sources* 426:33–39
- [42] Zhang W, Li J, Zhang J et al (2017) Top-down strategy to synthesize mesoporous dual carbon armored MnO nanoparticles for lithium-ion battery anodes. *ACS Appl Mater Interfaces* 9:12680–12686
- [43] Wu B, Xie Y, Meng Y et al (2019) Constructing unique heterogeneous cobalt-manganese oxide porous microspheres as anode for long-cycle and high-rate lithium ion batteries. *J Mater Chem A* 7:6149–6160
- [44] Guo Y, Feng T, Yang J et al (2019) MOF-derived manganese monoxide nanosheet assembled microflowers for enhanced lithium-ion. *Nanoscale* 11:10763–10773
- [45] Wang X, Ma L, Ji Q et al (2019) MnO/metal/carbon nanohybrid lithium-ion battery anode with enhanced electrochemical performance: universal facile scalable synthesis and fundamental understanding. *Adv Mater Interfaces* 6:1900335

Publisher's Note Springer Nature remains neutral with regard to jurisdictional claims in published maps and institutional affiliations.